

Photo-response enhancement in longitudinal porous GaN-based UV

Jing Li(李京), Shaolong Shi(师少龙), Yutong Chen(陈昱潼), Zhanhong Ma(马占红), Xia Li(李霞), Yang Liu(刘洋), and Tiangui Hu(胡天贵)

Citation: Chin. Phys. B, 2026, 35 (**4**): 048503. DOI: 10.1088/1674-1056/ae0018
http://cpb.iphy.ac.cn; http://iopscience.iop.org/cpb

What follows is a list of articles you may be interested in

Self-powered horizontally structured n-n heterojunction photodetector based on Si-GaN/β-Ga_2O_3 for UV detection

Muzi Li(李木子), Maolin Zhang(张茂林), Xueqiang Ji(季学强), Shan Li(李山), Lili Yang(杨莉莉), and Weihua Tang(唐为华)

Chin. Phys. B, 2026, 35 (**2**): 028502. DOI: 10.1088/1674-1056/adee8d

β-Ga_2O_3/BP heterojunction for deep ultraviolet and infrared narrowband dual-band photodetection

Zhichao Chen(陈志超), Feng Ji(季枫), Yadan Li(李亚丹), Yahan Wang(王雅涵), Xuehao Ge(葛薛豪), Kai Jiang(姜凯), Hai Zhu(朱海), and Xianghu Wang(王相虎)

Chin. Phys. B, 2025, 34 (**12**): 128501. DOI: 10.1088/1674-1056/adea9d

Self-powered broadband photodetector based on pyramid-structured Si/TiO_2 heterojunction

Leyao Wu(吴乐瑶), Xinnan Shi(师馨楠), Haibo Fan(范海波), Qiujie Li(李秋洁), Peng Hu(胡鹏), and Feng Teng(滕凤)

Chin. Phys. B, 2025, 34 (**8**): 088501. DOI: 10.1088/1674-1056/add50a

Review of a direct epitaxial approach to achieving micro-LEDs

Yuefei Cai(蔡月飞), Jie Bai(白洁), and Tao Wang(王涛)

Chin. Phys. B, 2023, 32 (**1**): 018508. DOI: 10.1088/1674-1056/ac90b5

Responsivity and noise characteristics of AlGaN/GaN-HEMT terahertz detectors at elevated temperatures

Zhi-Feng Tian(田志锋), Peng Xu(徐鹏), Yao Yu(余耀), Jian-Dong Sun(孙建东), Wei Feng(冯伟), Qing-Feng Ding(丁青峰), Zhan-Wei Meng(孟占伟), Xiang Li(李想), Jin-Hua Cai(蔡金华), Zhong-Xin Zheng(郑中信), Xin-Xing Li(李欣幸), Lin Jin(靳琳), Hua Qin(秦华), Yun-Fei Sun(孙云飞)

Chin. Phys. B, 2019, 28 (**5**): 058501. DOI: 10.1088/1674-1056/28/5/058501

Photo-response enhancement in longitudinal porous GaN-based UV

Jing Li(李京)[1,2], Shaolong Shi(师少龙)[1], Yutong Chen(陈昱潼)[4], Zhanhong Ma(马占红)[5], Xia Li(李霞)[1], Yang Liu(刘洋)[1,2], and Tiangui Hu(胡天贵)[1,2,3,†]

[1] *Yangtze Delta Region Institute (Quzhou), University of Electronic Science and Technology of China, Quzhou* 324003, *China*
[2] *State Key Laboratory of Electronic Thin Films and Integrated Devices, University of Electronic Science and Technology of China, Chengdu* 610054, *China*
[3] *State Key Laboratory of Superlattices and Microstructures, Institute of Semiconductors, Chinese Academy of Sciences, Beijing* 100083, *China*
[4] *Deepcreatic Technologies Ltd., Chengdu* 610000, *China*
[5] *School of Electronic and Electrical Engineering, Ningxia University, Yinchuan* 750021, *China*

(Received 4 June 2025; revised manuscript received 25 August 2025; accepted manuscript online 28 August 2025)

Gallium nitride (GaN), as a typical wide bandgap semiconductor, is an excellent candidate to fabricate the high-performance UV photodetector, due to its excellent intrinsic nature. However, the weak light absorption of conventional bulk GaN limits the further improvement of photo-response of GaN-based photodetectors. Here, we have prepared a longitudinal porous GaN using a simple electrochemical etching process, and then fabricated a porous GaN-based photodetector (Porous PD). The photo-response in the Porous PD has been improved significantly compared to the control planar GaN-based photodetector (Planar PD). At −1.2 V, the photo current (I_{photo}) in the Porous PD is ∼ 75 times higher than that of Planar PD, and the maximum responsivity of the Porous PD can reach 3.11×10^4 A/W, which is attributed to the large internal gain ($> 1.06 \times 10^5$). The maximum specific detectivity of the Porous PD has also been calculated to be 5.22×10^{13} Jones, two orders of magnitude higher than that of the Planar PD. Our work paves the way to develop high-performance GaN-based PDs for detecting weak optical signals.

Keywords: gallium nitride, nanopores, photodetector, electrochemical etching

PACS: 85.60.–q, 85.60.Bt, 85.60.Gz

DOI: 10.1088/1674-1056/ae0018 **CSTR:** 32038.14.CPB.ae0018

1. Introduction

Ultraviolet (UV) photodetection technique has been widely used in many advanced application fields, such as flame detection, space communication, environmental monitoring, and high-density photomemory, etc.[1–3] The key device to achieve UV photodetection is UV photodetector. Gallium nitride (GaN), as a typical wide bandgap semiconductor, is an excellent candidate to fabricate the high-performance UV photodetector, due to its excellent intrinsic nature,[4–6] such as direct wide bandgap (UV absorption window), high breakdown voltage, superior radioresistance, high electron saturation drift velocity, high chemical and thermal stability, etc. Until now, many kinds of GaN-based UV photodetectors have been reported,[7–9] including pin photodetector, and metal–semiconductor–metal (MSM) photodetector. Among them, the MSM structure has drawn lots of attention because of its advantages,[10,11] such as easy to fabricate and integrate, low electric capacity, etc. However, due to the weak light absorption of bulk GaN, the traditional GaN-based MSM UV photodetectors exhibit a low responsivity of 1.31 A/W,[12] indicating a low photo-response.

An alternative approach to improve the photo-response of GaN-based photodetector is to introduce nanostructures,[13–15] which has larger surface-to-volume ratio and the light modulation effect.[16–18] Larger surface-area-to-volume ratio can significantly increase the light absorption, resulting in the enhancement of the photo current and photo-gain,[19] while the light modulation from the nanostructure itself can 'trap' the incident light entering the interior of GaN, leading to the improvement of the light absorption. In addition, the formation of nanostuctures can not only improve the light absorption of GaN film, but also induce a lot of surface defects and dangling bonds. These surface defects and dangling bonds serve as the trap centers to capture/emit photo-generated carriers (trapping effect), which would significantly prolong the lifetime of the photo-generated carriers, resulting in a larger photo-gain.[20,21]

So far, various types of nanostructured GaN have been demonstrated in past decades,[22–24] including nanocolumns GaN, silver-decorated GaN, nanorod GaN, etc. Nevertheless, the fabrication methods adopted in these works are top-down etching methods and need to prepare masks before etching,[22–25] either aluminum oxide (AAO) membranes or rapid thermal annealing metals, which makes the whole fabrication process more complicated and largely increases the time and cost spent on the process. Different from these nanos-

†Corresponding author. E-mail: tghu@csj.uestc.edu.cn

© 2026 Chinese Physical Society and IOP Publishing Ltd. All rights, including for text and data mining, AI training, and similar technologies, are reserved.

tructrues, nanoporous GaN can be fabricated using a simple electrochemical etching process, reducing the preparation cost.

Here, we have fabricated a longitudinal porous GaN using a simple electrochemical etching process, which largely reduces the complexity and cost for fabricating nanostructured GaN. The SEM images show that the pores density and porosity in the porous GaN are calculated to be 3.75 μm^{-2} and 0.83%, respectively, and the average diameter of the pore channels is $\sim$ 49.5 nm. The PL peak position of the porous GaN (363.28 nm) exhibits a slightly red shift compared to that of the planar GaN (363.19 nm), which is attributed to the strain relaxation after formation of lots of nanopores verified by Raman spectra. The photo-response in the Porous PD has been improved significantly compared to the control Planar PD. At -1.2 V, the photo current (I_{photo}) in the Porous PD is $\sim$ 75 times higher than that of the planar GaN-based photodetector (Planar PD), and the maximum responsivity of the Porous PD can reach $3.11.\times10^4$ A/W, which is attributed to the large internal gain ($> 1.06 \times 10^5$). The maximum specific detectivity of the Porous PD has also been calculated to be 5.22×10^{13} Jones, two orders of magnitude higher than that of the Planar PD. This high performance GaN-based PDs lay a foundation for detecting weak UV optical signals.

2. Experimental details

2.1. Fabrication of the longitudinal porous GaN

The whole GaN epitaxial structure consists of a *c*-plane sapphire substrate, a 30-nm-thick nucleation layer, and a 3-μm-thick Si-doped GaN layer. The epitaxy technique was metal–organic chemical vapor deposition, with high purity trimethylgallium and ammonia as the precursors, hydrogen as the carrier gas.[26,27] The Hall measurement results show that the specific doping concentration of the Si-doped GaN layer is 3×10^{18} cm^{-3}. Afterwards, the as-grown GaN piece served as the anode and immersed into the 1-mol/L NaOH solutions together with a Pt cathode. Under an applied voltage of 30 V, partial GaN was oxidized and dissolved after 5 min, and the related chemical reactions are as follows:

$$2GaN + 6H_2O + 6h^+ \rightarrow Ga(OH)_3 + N_2 + 6H^+, \quad (1)$$

$$Ga(OH)_3 + OH^- \rightarrow GaO_2^- + 2H_2O. \quad (2)$$

Finally, the as-grown GaN piece was picked out from the electrolyte solution and cleaned in the deionized water. After dried by the N_2 gun, the fabrication of the porous GaN was completed, and the schematic fabrication diagram is shown in Fig. S1 of the supporting information.

2.2. Fabrication of the longitudinal porous GaN-based photodetector

Based on the preparation of the porous GaN, the corresponding porous GaN-based photodetector (Porous PD) was fabricated, and for comparison, we also fabricated planar GaN-based photodetector (Planar PD) as reference. The electrode pattern was designed to be interdigital pattern to collect photo-generated carriers more efficiently, which was defined by lithography technology.[28] The electrode materials were 50 nm-thick Ti and 250-nm-thick Au, and the deposition technique was magnetron sputtering. The length and width of the interdigital fingers are 285 μm and 10 μm with the space of 10 μm, and the active area of the photodetectors is 300 μm×400 μm, as shown in Fig. S2 of the supporting information.

2.3. Measurements

FEI NanoSEM650 was used to take the SEM pictures and observe the morphology of the porous GaN and the planar GaN. High-Resolution Raman Imaging System (Renishaw inVia-Qontor) was used to measure the photoluminescence (PL) and Raman spectra, and the corresponding laser wavelengths were 325 nm and 532 nm, respectively. An optoelectronic measurement system, consisting of an Agilent semiconductor parameter analyzer B1500A to collect *I*–*V* data, a 150-W Xe lamp served as light source, an Omniλ300 monochromator to tune the light wavelength, and a calibrated power meter Thorlabs GmbH. PM 100D to measure the light power, was assembled to measure the *I*–*V* characteristics of the Porous PD and the Planar PD.

3. Results and discussion

3.1. Characterization of the longitudinal porous GaN

Figures 1(a) and 1(b) show the top-view SEM images of the planar and porous GaNs. Compared to the planar GaN, lots of pores appear on the surface of the porous GaN, which can be illustrated as follows. Due to the heteroepitaxy, there are a lot of surface defects in the GaN film grown on sapphire substrate. When applied voltages, these defects with high chemical activity will oxide and dissolute during electrochemical etching, resulting in the formation of surface pores. Because of the random distribution of defects, the positions of the formed surface pores are also randomly distributed. The more detailed illustration about the formation of these pores can be referred in our previous works.[29–32] We have conducted statistics on the pore area distribution in the top-view SEM image of the Porous GaN using Image-Pro Plus software, as shown in Fig. S3. The number, the mean area, the pores density, and porosity of the nanopores are calculated to be 178, 0.0022 μm^2, 3.75 μm^{-2}, and 0.83%, respectively. Figures 1(c) and 1(d) show the corresponding cross-sectional SEM images of the planar and porous GaNs. It can be seen clearly that the pore channels have already penetrated through the entire n-GaN film in the porous GaN, and the average diameter of the pore channels is $\sim$ 49.5 nm.

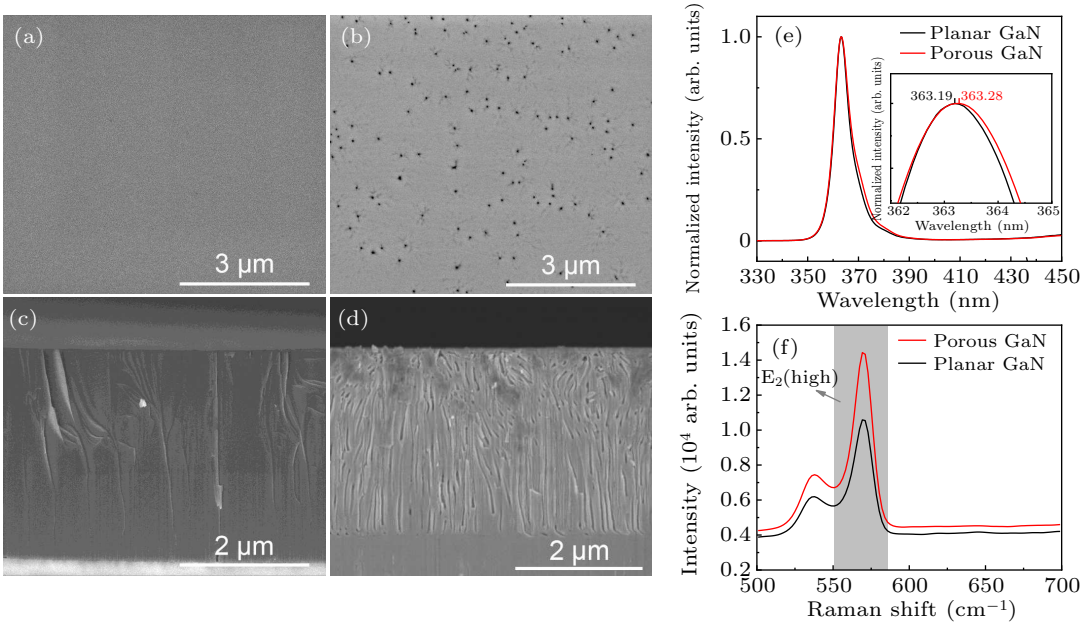


Fig. 1. Top-view SEM images of (a) the planar GaN and (b) the porous GaN, respectively. Cross-sectional SEM images of (c) the planar GaN and (d) the porous GaN, respectively. (e) Photoluminescence and (f) Raman spectra of the planar and porous GaNs.

To investigate the physical properties of GaN film before and after the formation of nanopores, we measured the photoluminescence (PL) spectra of the planar and porous GaNs, as shown in Fig. 1(e). The full width at half maximum (FWHM) of the porous GaN is 7.94 nm, slightly wider than that of the planar GaN (7.16 nm), which is attributed to more surface defects in the porous GaN. During electrochemical etching process, the dissolution of GaN molecules not only forms nanopores, but also leaves lots of dangling bonds and surface defects.[33] The PL peak position of the porous GaN is 363.28 nm, exhibiting a slightly red shift compared to that of the planar GaN (363.19 nm), which is attributed to the strain relaxation after formation of lots of nanopores.[34,35] Due to the heteroepitaxy, there are a lot of compressive stresses in the GaN film grown on sapphire substrate, which increases the energy bandgap of the GaN film.[36] After electrochemical etching, lots of nanopores are formed in the GaN film, and the residual compressive stresses can be relaxed, resulting in the decrease of the energy bandgap and the slightly red shift of the PL peak.[34,35]

The strain change can be verified using Raman measurement, as shown in Fig. 1(f). Compared to the planar GaN (569.41 cm^{-1}), the E_2(high) phonon peak of the porous GaN shifts to 569.24 cm^{-1}, indicating a compressive strain relaxation, which is consistent with the PL measurement result.[32,36] The specific relaxation strain can be calculated to be 0.04 GPa using the following equation:[37]

$$\sigma = \frac{\Delta\omega}{4.3\ (\ \mathrm{cm}^{-1}\cdot\mathrm{GPa}^{-1})},$$

where σ represents the biaxial stress and $\Delta\omega$ is the relative shift of E_2(high) phonon peaks. We also measured the reflectivity spectra of the planar and porous GaNs, as shown in Fig. S4. Compared to the planar GaN, the reflectivity of the porous GaN decreases significantly, and at 363 nm, the specific reflectivity of the porous GaN is 15.9%, more than 2 times lower than that of the planar GaN (41.1%). The lower reflectivity indicates a stronger light absorption in the porous GaN, which is attributed to the larger surface-area-to-volume ratio of nanopores. To exclude the effect of the band gap of material, we simulated the reflectivity of the porous metal Cu, as shown in Fig. S5. Compared with the bulk Cu, the reflectivity of the porous metal Cu decreases significantly, consistent with the reflectivity of the porous GaN, which indicates that the higher photocurrent is attributed to the light trapping effect of the porous nanostructure and no involvement of band gap of the material.

3.2. Performance of the longitudinal porous GaN-based photodetector

3.2.1. Photo and dark current

Based on the preparation of the nano-porous GaN film, the corresponding MSM UV photodetector (Porous PD) with symmetric Au/Ti/GaN/Ti/Au structure was fabricated, and for comparision, a planar GaN-based photodetector with the same structure (Planar PD) was also prepared. The schematic diagrams of these two devices are shown in Figs. 2(a) and 2(b). Figure 2(c) shows the *I*–*V* characteristics of the Planar PD and Porous PD under dark condition. At −5 V, the dark current (I_{dark}) of the Porous PD is 1.83 mA, lower than that of the Planar PD (11.50 mA), which is attributed to the reduction of the background carrier density following the conversion of n^+-GaN film into a nanopores structure.[38] Meanwhile, it can be seen clearly that the current increasing rate with voltage in the Porous PD is lower than that of the Planar PD, which can be

illustrated as follows. According to the thermionic emission theory, when the influence the influence of image force and tunneling on the height of Schottky barrier were ignored, the relationship between dark current ($I_{\rm dark}$) and applied voltage (V) is as follows:

$$I_{\rm dark} = AA^*T^2 \exp\left(-\frac{\phi_{\rm B}}{nkT}\right)\left(\exp\frac{qV}{nkT} - 1\right), \tag{3}$$

where A, A^*, T, $\phi_{\rm B}$, n, k, and q are the area of electrodes, the Richardson constant, the temperature, the Schottky barrier in the device, ideal factor, the Boltzmann constant, and the elementary charge, respectively. At room temperature,

$$kT \approx 0.026\ \text{eV} \ll qV, \tag{4}$$

therefore,

$$\exp\frac{qV}{nkT} \gg 1. \tag{5}$$

Equation (3) can be simplified to be

$$I_{\rm dark} = AA^*T^2 \exp\left(\frac{qV - \phi_{\rm B}}{nkT}\right), \tag{6}$$

taking the logarithm of both sides, equation (6) can be transformed into

$$\lg I_{\rm dark} = \lg AA^*T^2 + \frac{qV - \phi_{\rm B}}{nkT}, \tag{7}$$

from Eq. (7), we can conclude that the current increasing rate with voltage in Fig. 2(c) is linearly dependent on the coefficient q/nkT. Due to the formation of nanopores using electrochemical etching, there are lots of dangling bonds and surface defects in the Porous PD, resulting in a higher ideal factor (n) than the Planar PD. Therefore, the current increasing rate with voltage in the Porous PD is lower than that of the Planar PD.

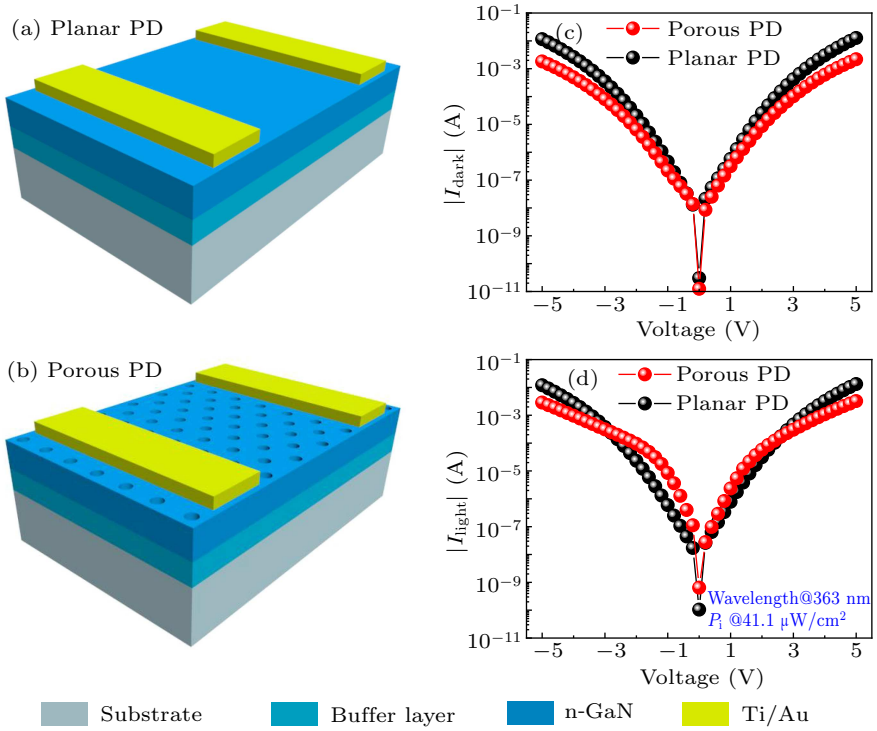


Fig. 2. Schematic diagrams of (a) the Planar PD and (b) the Porous PD. (c) *I*–*V* curves of the planar and porous PDs under dark condition. (d) *I*–*V* curves of the planar and porous PDs, with the illumination power density of 41.1 μW/cm^2 and the illumination wavelength of 363 nm.

Figure 2(d) shows the *I*–*V* characteristics ($I_{\rm light}$) of the Planar PD and Porous PD under light condition, with the illumination power density of 41.1 μW/cm^2 and the illumination wavelength of 363 nm. At low voltage, the light current ($I_{\rm light}$) in the Porous PD is higher than that in the Planar PD, while they are reverse at high voltages. This phenomenon is mainly because the light current consists of two parts: dark current ($I_{\rm dark}$) and photo current ($I_{\rm photo}$), respectively. At low voltage, the dark current ($I_{\rm dark}$) is so low that can be neglected, and the photo current ($I_{\rm photo}$) is dominant in the overall light current ($I_{\rm light}$). Compared to the Planar PD, the Porous PD has stronger light absorption due to the larger surface-area-to-volume ratio, resulting in a higher photo current ($I_{\rm photo}$) and light current ($I_{\rm light}$). At high voltage, the dark current ($I_{\rm dark}$) is so high that the photo current ($I_{\rm photo}$) can be neglected, leading to a lower light current ($I_{\rm light}$) in the Porous PD. At −1.2 V, the photo current ($I_{\rm photo}$) in the Porous PD is 17.30 μA, ∼ 75 times higher than that of the Planar PD (0.23 μA).

The illumination power density dependent light current ($I_{\rm light}$) of the Porous PD has also been measured, as shown in Fig. S6. The light current ($I_{\rm light}$) is positively relative to the illumination power density ($P_{\rm i}$) and follows the power law: $I_{\rm Light} \propto P_{\rm i}^{\alpha}$, where the index α is related to the recombination probability of photo-generated carriers,[39,40] as shown in

Fig. S7. Affected by the surface defects and states, the number of recombination centers in the Porous PD increases, causing the specific value of α is calculated to be 0.48, less than 1.

3.2.2. Responsivity and specific detectivity

Based on the measurement results of the light and dark current, the corresponding photo-responsivities (R) of the Planar PD and the Porous PD at different voltages can be calculated, as shown in Fig. 3(a). The responsivities for the Planar PD and the Porous PD increase with increasing the applied voltages, which reach the maximum value of 1.29×10^4 A/W and 3.11×10^4 A/W at -5 V, respectively. Otherwise, the responsivity of the Porous PD is significantly higher than that of the Planar PD, and at -1.2 V, the corresponding improvement ratio reaches the maximum value, ~ 75, as shown in Fig. S8. The higher responsivity is corresponding to a higher internal gain (G). According to the equation $R = G\eta(\lambda e/hc)$,[21] where h, c, λ, e, and η are the Planck constant, the light speed, the illumination wavelength, the elementary charge, and the internal quantum efficiency, respectively, the product $G\eta$ can be calculated, as shown in Fig. 3(b), and the specific values of the Porous PD at -5 V is 1.06×10^5. Since $\eta < 100\%$, the corresponding internal gains (G) are higher than 1.06×10^5.

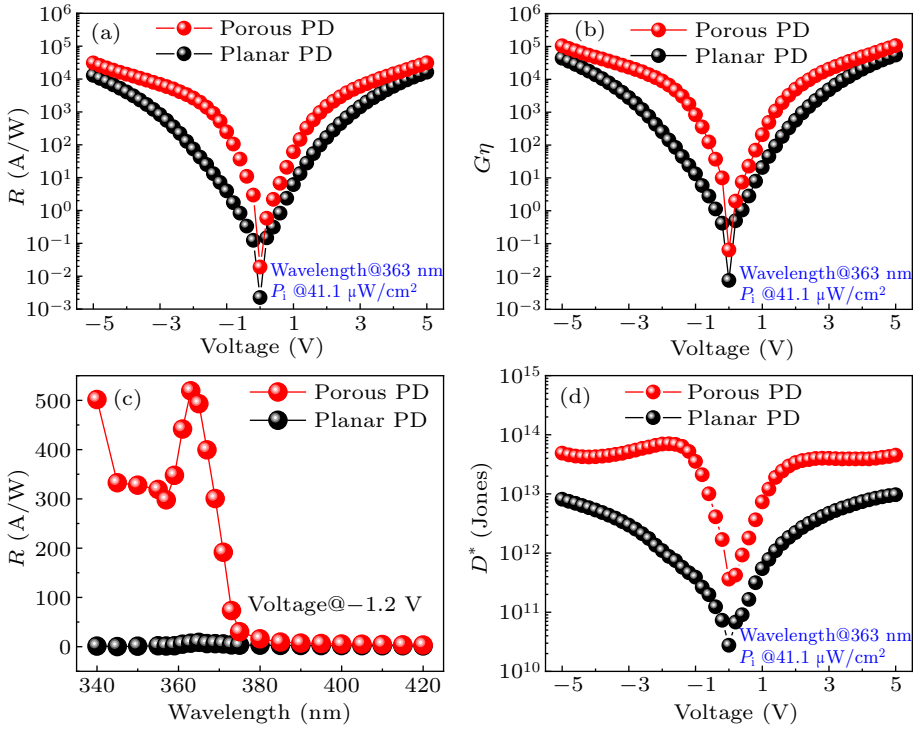


Fig. 3. (a) Responsivity of the Planar PD and the Porous PD at different applied voltages. (b) The product of the internal gain and quantum efficiency in the Planar PD and the Porous PD. (c) Wavelength-dependent responsivity of the Planar PD and the Porous PD at -1.2 V. (d) The corresponding specific detectivity of the Planar PD and the Porous PD, with the illumination power density of 41.1 μW/cm^2 and the illumination wavelength of 363 nm.

There are several mechanisms to illustrate the high internal gain (G), including avalanche carrier multiplication at high electric fields, photoconductive gain, and trapping effect.[21] In our device, the trapping effect is the dominant factor. The formation of nanopores can not only improve the light absorption of GaN film, but also induce a lot of surface defects and dangling bonds. These surface defects and dangling bonds serve as the trap centers to capture/emit photo-generated carriers (trapping effect), which would significantly prolong the lifetime of the photo-generated carriers, resulting in a larger gain according to the equation $G = \tau_{\text{lifetime}}/\tau_{\text{transit}}$, where τ_{lifetime} and τ_{transit} represent the lifetime and the transit time of the photo-generated carriers, respectively.[41,42]

To investigate the wavelength selectivity, we also plotted the wavelength-dependent photo-responsivities of the Planar PD and Porous PD, as shown in Fig. 3(c). The rejection ratio of the Planar PD and Porous PD, defined as $R(363\text{ nm})/R(400\text{ nm})$, are 3.4 and 102.1 at -1.2 V, respectively, indicating that the Porous PD not only exhibits higher photo-responsivity, but also has a better wavelength selectivity.

The specific detectivity (D^*) is an important characteristic for photodetectors, which describes the smallest detectable optical signal and can be expressed as[43,44]

$$D^* = \frac{R}{\sqrt{2eJ_{\text{dark}}}}, \tag{8}$$

where e is the elementary charge, R and J_{dark} represent the responsivity and the dark current density, respectively. Figure 3(d) shows the corresponding specific detectivity of the Planar PD and Porous PD. Attributed to the higher photo current and lower dark current, the detectivity of the Porous PD is

improved significantly compared to the Planar PD. At −1.2 V, the specific detectivity of the Porous PD is 5.22×10^{13} Jones, two orders of magnitude higher than that of the Planar PD, which indicates a more excellent detectability for weak optical signal in the Porous PD.

3.2.3. Response time

We have built a measurement system consisting of a signal generator, current preamplifier, oscilloscope and an LED light source with a central wavelength of 365 nm to define the response time of the Porous PD and the control Planar PD, as shown in Fig. S9. By calculating the consumed time from 10% (90%) to 90% (10%) of the maximum current value,[42,45] the rise time (τ_r) and decay time (τ_d) of the Porous PD are 45.6 ms and 51.2 ms, respectively, slightly slower than that of the Planar PD (19.2 ms/ 20.4 ms), which is mainly attributed to trapping effects.[21] After electrochemical etching, a large number of defects existed in nanopores serve as trapping centers to capture and emit photo-generated carriers (trapping effect), which would prolong the whole response time of photo-generated carriers.

3.3. Mechanism of the enhanced properties

Compared to the planar GaN, the porous GaN has larger surface-to-volume ratio, leading to a stronger light absorption and more photo-generated carriers. On the other hand, the light modulation from the porous nanostructure itself plays an important role in the enhancement of the optoelectronics properties. Because of the existence of these pores, the optical field in the porous GaN is re-distributed, and a large amount of incident light is trapped into the porous nanostructure, resulting in the reduction of the reflectance. To further understand the light modulation phenomenon, we simulated the optical field distribution ($\log|E|$) of the planar GaN and the porous GaN, respectively, using FDTD solutions, as shown in Fig. 4. It can be seen clearly that the incident light is confined inside the porous GaN. The larger surface-to-volume ratio and light-modulation effect can improve the efficiency of the light utilization and thus enhance the photo current.[18]

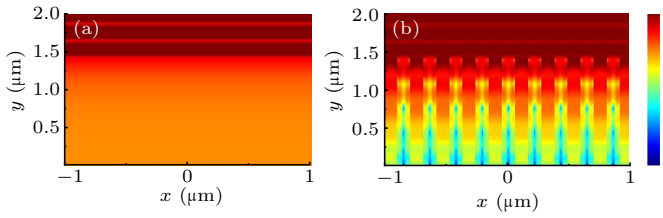


Fig. 4. Simulated optical field distribution of (a) the planar GaN and (b) the porous GaN.

4. Conclusion

In summary, we have fabricated a longitudinal porous GaN using a simple electrochemical etching process, which largely reduces the complexity and cost for fabricating nanostructured GaN. The SEM images show that the pores density and porosity in the porous GaN are calculated to be 3.75 μm^{-2} and 0.83 %, respectively, and the average diameter of the pore channels is ∼ 49.5 nm. The PL peak position of the porous GaN (363.28 nm) exhibits a slightly red shift compared to that of the planar GaN (363.19 nm), which is attributed to the strain relaxation after formation of lots of nanopores verified by Raman spectra. The photo-response in the Porous PD has been improved significantly compared to the control Planar PD. At −1.2 V, the photo current (I_{photo}) in the Porous PD is ∼ 75 times higher than that of the planar GaN-based photodetector (Planar PD), and the maximum responsivity of the Porous PD can reach 3.11×10^4 A/W, which is attributed to the large internal gain ($> 1.06\times10^5$). The maximum specific detectivity of the Porous PD has also been calculated to be 5.22×10^{13} Jones, two orders of magnitude higher than that of the Planar PD. Our work suggests that the porous nanostructure can significantly improve the light absorption and the photo-response of GaN-based PDs, providing a new approach to fabricate high-performance GaN-based PDs for detecting weak optical signals.

Acknowledgements

Project supported by the Joint Fund of the Zhejiang Provincial Natural Science Foundation of China (Grant No. LQZQN25F050001), the Fund from the Municipal Government of Quzhou City, China (Grant Nos. 2023D021, 2024D014, and 2023D031), the National Natural Science Foundation of China (Grant No. 62472322), and the Central Leading Local Science and Technology Development Fund Project (Grant No. 2024FRD05005).

References

[1] Xu X J, Chen J X, Cai S, Long Z H, Su L X, He S S, Tang C Q, Liu P, Peng H S and Fang X S 2018 *Adv. Mater.* **30** 1803165
[2] Li S, Guo D Y, Li P G, Wang X, Wang Y H, Yan Z Y, Liu Z, Zhi Y S, Huang Y J, Wu Z P and Tang W H 2019 *ACS Applied Materials & Interfaces* **11** 35105
[3] Ouyang W X, Teng F, He J H and Fang X S 2019 *Adv. Funct. Mater.* **29** 1807672
[4] Monroy E, Calle F, Muñoz E and Omnès F 1999 *Appl. Phys. Lett.* **74** 3401
[5] Zhang X L, Liu B D, Liu Q Y, Yang W J, Xiong C M, Li J and Jiang X 2016 *ACS Applied Materials & Interfaces* **9** 2669
[6] Golgir H R, Li D W, Keramatnejad K, Zou Q M, Xiao J, Wang F, Jiang L, Silvain J F and Lu Y F 2017 *ACS Applied Materials & Interfaces* **9** 21539
[7] Parish G, Keller S, Kozodoy P, Ibbetson J P, Marchand H, Fini P T, Fleischer S B, DenBaars S P, Mishra U K and Tarsa E J 1999 *Appl. Phys. Lett.* **75** 247
[8] Chen Q, Yang J W, Osinsky A, Gangopadhyay S, Lim B, Anwar M Z, Khan M A, Kuksenkov D and Temkin H 1997 *Appl. Phys. Lett.* **70** 2277
[9] Gundimeda A, Krishna S, Aggarwal N, Sharma A, Sharma N D, Maurya K K, Husale S and Gupta G 2017 *Appl. Phys. Lett.* **110** 103507

[10] Monroy E, Calle F, Pau J L, Muñoz E, Omnès F, Beaumont B and Gibart P 2001 *Journal of Crystal Growth* **230** 537

[11] Chui C O, Okyay A K and Saraswat K C 2003 *IEEE Photon. Technol. Lett.* **15** 1585

[12] Li D B, Sun X J, Song H, Li Z M, Jiang H, Chen Y R, Miao G Q and Shen B 2011 *Appl. Phys. Lett.* **99** 261102

[13] Wang X F, Zhang Y, Chen X M, He M, Liu C, Yin Y, Zou X S and Li S T 2014 *Nanoscale* **6** 12009

[14] Nasiri N, Jin D and Tricoli A 2018 *Adv. Opt. Mater.* **7** 1800580

[15] Hatch S M, Briscoe J and Dunn S 2012 *Adv. Mater.* **25** 867

[16] Li J, Xi X, Li X D, Lin S, Ma Z H, Xiu H X and Zhao L X 2020 *Adv. Opt. Mater.* **8** 1902162

[17] Li J K, Qiu Y C, Wei Z H, Lin Q F, Zhang Q P, Yan K Y, Chen H N, Xiao S, Fan Z Y and Yang S H 2014 *Energy Environ Sci* **7** 3651

[18] Hou W and Cronin S B 2013 *Adv. Funct. Mater.* **23** 1612

[19] Nasiri N, Bo R, Fu L and Tricoli A 2017 *Nanoscale* **9** 2059

[20] Hu T G, Li X D, Liu C, Lin S, Wang K Y, Liu J and Zhao L X 2022 *J. Phys. D: Appl. Phys.* **55** 035102

[21] Liu L, Yang C, Patanè A, Yu Z G, Yan F G, Wang K Y, Lu H X, Li J M and Zhao L X 2017 *Nanoscale* **9** 8142

[22] Benton J, Bai J and Wang T 2013 *Appl. Phys. Lett.* **102** 173905

[23] Hou Y, Syed Z A, Smith R, Athanasiou M, Gong Y, Yu X, Bai J and Wang T 2016 *J. Phys. D: Appl. Phys.* **49** 265601

[24] Xi X, Yang C, Cao H C, Yu Z G, Li J, Lin S, Ma Z H and Zhao L X 2018 *Appl. Surf. Sci.* **462** 310

[25] Li Z P, Xu Z M, Li D J, Wu A X and Ruan R L 2019 *J. Alloys Compd.* **803** 748

[26] Hardtdegen H, Hollfelder M, Meyer R, Carius R, Münder H, Frohnhoff S, Szynka D and Lüth H 1992 *Journal of Crystal Growth* **124** 420

[27] Cho Y S, Hardtdegen H, Kaluza N, Thillosen N, Steins R, Sofer Z and Lüth H 2006 *Physica Status Solidi C* **3** 1408

[28] Khan M A, Kuznia J N, Olson D T, Van Hove J M, Blasingame M and Reitz L F 1992 *Appl. Phys. Lett.* **60** 2917

[29] Li X D, Yang C, Li J, Xi X, Ma Z H, Lin S and Zhao L X 2020 *Appl. Surf. Sci.* **526** 146618

[30] Li X D, Hu T G, Lin S, Ma Z H, Wang J F and Zhao L X 2021 *International Journal of Hydrogen Energy* **46** 7878

[31] Yang C, Liu L, Zhu S C, Yu Z G, Xi X, Wu S T, Cao H C, Li J M and Zhao L X 2017 *J. Phys. Chem. C* **121** 7331

[32] Hu T G, Liu C and Liu J 2022 *J. Electrochem. Soc.* **169** 066514

[33] Pajot B and Clerjaud B 2013 *Springer Series in Solid-State Sciences* pp. 43–88

[34] Kornienko N, Gibson N A, Zhang H, Eaton S W, Yu Y, Aloni S, Leone S R and Yang P 2016 *ACS Nano* **10** 5525

[35] Wang S Z, Zhang L, Sun C L, Shao Y L, Wu Y Z, Lv J X and Hao X P 2016 *Adv. Mater.* **28** 3768

[36] Zhao D G, Xu S J, Xie M H, Tong S Y and Yang H 2003 *Appl. Phys. Lett.* **83** 677

[37] Landmann M, Rauls E, Schmidt W G, Neumann M D, Speiser E and Esser N 2015 *Phys. Rev. B* **91** 035302

[38] Zhang C, Park S H, Chen D, Lin D W, Xiong W, Kuo H C, Lin C F, Cao H and Han J 2015 *ACS Photon.* **2** 980

[39] Wei X, Yan F G, Lv Q S, Zhu W K, Hu C, Patanè A and Wang K Y 2019 *Adv. Opt. Mater.* **7** 1900190

[40] Yan F G, Zhao L X, Patanè A, Hu P A, Wei X, Luo W G, Zhang D, Lv Q S, Feng Q, Shen C, Chang K, Eaves L E and Wang K Y 2017 *Nanotechnology* **28** 27

[41] Xie S H, Dey A, Yan W J, Kudrynskyi Z R, Balakrishnan N, Makarovsky O, Kovalyuk Z D, Castanon E G, Kolosov O, Wang K Y and Patanè A 2021 *2D Mater.* **8** 2053

[42] Jie J S, Zhang W J, Jiang Y, Meng X M, Li Y Q and Lee S T 2006 *Nano Lett.* **6** 1887

[43] Gong X, Tong M H, Xia Y J, Cai W Z, Moon J S, Cao Y, Yu G, Shieh C L, Nilsson B and Heeger A J 2009 *Science* **325** 1665

[44] Hao L Z, Gao W, Liu Y J, Liu Y M, Han Z D, Xue Q Z and Zhu J 2016 *Phys. Chem. Chem. Phys.* **18** 1131

[45] Kaushik S and Singh R 2021 *Adv. Opt. Mater.* **9** 2002214